Deuterium blistering and retention in tungsten vanadium alloys

Kameel Arshad[a], Yue Yuan[a,*], Long Cheng[a], Jun Wang[a], Zhang-Jian Zhou[b,*], G. De Temmerman[c], Xiang Liu[d], Guang-Nan Luo[e], Guang-Hong Lu[a,*]

[a]*School of Physics and Nuclear Energy Engineering, Beihang University, Beijing 100191, China*

[b]*School of Materials Science and Engineering, University of Science and Technology Beijing (USTB), Beijing 100083, China*

[c]*FOM Institute for Plasma Physics, Edisonbaan 14, 3439 MN Nieuwegein, Netherlands*

[d]*South West Institute of Physics (SWIP), Sichuan, China*

[e]*Institute of Plasma Physics, Chinese Academy of Sciences (ASIPP), Hefei 230031, China*

Abstract

In order to evaluate D blistering and retention behavior in W based plasma facing materials, different grades of W-V targets were exposed to high flux of $1.2 \times 10^{24}\ m^{-2}s^{-1}$, low energy (38 eV) D plasma at two different temperatures. The blistering behavior was investigated by means of scanning electron microscopy, accompanied by electron back-scattering diffraction and focused ion beam, where thermal desorption spectroscopy was used to study the D retention from the tested samples. The addition of both kinds of V precursor to W suppressed D blistering formation. Comparatively submicron V-containing materials have shown high tendency but small size blisters formation than micron V-containing samples. High dense blisters were observed near (111) plane on the surface of submicron V-containing alloys. Nano-sized blisters were also observed on V enriched surface. No blisters were observed on the grain boundaries and the diffused V particles in W were not responsible for D blistering formation. Lower D retention was

found for submicron V-containing targets as compared to micron V-containing samples, at both irradiated temperatures. It was noted that the increase in surface temperature of the irradiated target, leads to a slight shift of the desorption peaks toward higher temperatures and increase the net amount of retained D. For same kind of samples, the D blistering and retention was higher for higher irradiated temperatures.

PACS: (53.40.Hf.81.05.Bx)

Keywords: Tungsten-vanadium alloy; deuterium plasma; retention; blistering

1. Introduction

The main handle for the development and a viable operation of fusion power reactor is the selection of plasma facing materials (PFMs). W due to its durability and favorable physical properties at elevated temperatures is considered as a choice for a plasma facing material (PFM) in an advanced fusion reactor[1-5]. However, one of the drawbacks of W is its high ductile-to-brittle transition temperature (DBTT)[6].

W as a divertor of fusion reactor face high heat flux up to 10 MWm^{-2} and high particle flux including neutron, helium (He) and hydrogen (H) up to 10^{24} $m^{-2}s^{-1}$, while loads at other plasma-facing walls can be orders of magnitude smaller[7]. These loads on W, change its morphology of the surfaces and largely degrade the physical and mechanical properties. This issue demands to develop new W based alloys with improved ductility and other properties for fusion environment. A lot of research is going on to develop and characterize W based materials with improved properties and microstructures, which can withstand against the intense environment of fusion

reactor[8-17].

Limited numbers of elements form solid solution and have significant solubility in W at room temperature. Only few of them do not form brittle intermetallic compounds with W. Only Ta, V, Nb and Mo has a full rang solvability in W, besides these, a few, e.g., Ti and Re have a limited solubility. Their applicability is constrained to fractions of about 12% and 27%, respectively, due to the formation of intermetallic σ- and χ-phases[18, 19]. Re is the only known alloying metal used for ductilization of W by solid solution[20]. Rest of the mentioned metals also form solid solution but they can't reduce DBTT of W based materials. For plasma facing materials, Re addition to W is avoided due to its activation and formation of brittle phases due to significant transmutation of Re into Os[21]. Similarly, applicability of Nb and Mo is doubted for fusion applications because they transmute to very long-lived radioactive isotopes[22]; this leaves Ta, V, and Ti as possible alloying elements for W based materials. Recent studies of W-Ti alloys, fabricated with different route, was failed to promote promising results[23, 24]. The formation of metastable Ti phases is responsible for poor the mechanical properties of W–Ti alloys. The fracture toughness of the W based materials decreases with the increase of Ta concentration[25].

However, our recent studies suggest that the addition of V in W constrains the grain growth and improves the densification and mechanical properties[26]. Fine-grained W materials have shown attractive properties in terms of reduction in brittleness and improvement in toughness and strength [27, 28]. The fracture toughness of the alloys is gradually increased with the increase of V concentration[26]. Furthermore, the V precursor's powder size also plays an important role in the grain refinement and improvement of mechanical properties of the fabricated W-V alloys. The addition of

submicron V precursor highly improved mechanical properties including micro-harness and fracture toughness of W based alloys as compared to micron V precursor. Similarly a large refinement of W grains can be achieved by adding submicron V precursor[29]. However, the mechanical properties of plasma facing materials at higher temperatures (higher than the recrystallization temperature) for long time are highly deteriorated [27, 28]. V addition also enhances the thermal stability of the microstructures and mechanical properties of W-based materials[30]. Moreover, V shows high stability against the activation and transmutation under neutron irradiation as compared to W, Re, Ta etc. [31].

Change of the material microstructures and composition due to neutron transmutation can influence hydrogen trapping in W. V addition provides stability to W microstructures and reduces its degradation against neutron. Until now, there is no experimental study available on the subject of D implantation in different grades W-V alloys. The present work is performed to obtain important information about on D accumulation due to the influence of different V precursor admixture with W.

2. Experimental procedure

2.1. Target materials

SPS fabricated W-V alloys with different precursor particle size of V, micron-size (WVm) and submicron size (WVs) at 5 wt.% of V were mixed with W in planetary ball miller. The average precursor particle of micron and submicron V powder was 48 μm and 0.8 μm respectively, where 2 μm powder size was used for W. The powder mixing technique and SPS sintering conditions were discussed in our previous work[26]. Commercially available fully recrystallized rolled W samples were also tested for comparison. The

surface of each sample was mechanically polished with mirror finish. Due to short dwell time of 3 min at peak sintering temperature of 1873 K, relative low grain growth took place and the average grain size of WVm and WVs was ~ 2.4 μm and 1.8 μm respectively.

2.2. Experimental setup

A linear plasma generator Pilot-PSI in FOM Institute for Plasma Physics (Netherlands) was used for this investigation, capable of delivering low energy, high flux D plasma to simulate ITER like conditions. The detailed design and parameters of Pilot-PSI for D irradiation has been reported by M. H. J. t. Hoen et al[32]. The ion beam distribution on the target surface has been discussed by Zayachuk et al[15]. The incident D plasma energy and flux were set to 38 eV and ~ 1.2×10^{24} $m^{-2}s^{-1}$ respectively. The predominant ion species was D^+. The ion energy was determined from the bias voltage and the plasma potential measured by a Langmuir probe. Two different surface temperatures 453 K and 573 K were used for comparison, which were monitored by an infrared camera. The irradiation parameters of the target samples are tabulated in Table 1. Morphology of D blistering behavior of the investigated materials was analyzed with different techniques, such as scanning electron microscopy (SEM), electron back-scattering diffraction (EBSD) and focused ion beam (FIB), where thermal desorption spectroscopy (TDS) at a ramp rate of 0.5 K s^{-1} was used to study the D retention from the tested samples. A standard D leak with accuracy higher than 90% was used to calibrate the mass spectrometer prior to each TDS analysis.

Table 1: Deuterium plasma exposure conditions for different W-V targets.

Samples	Porosity level (%)	Deuterium fluence ($\times 10^{26}$ D m^{-2})	Surface temperature (K)
W	~0.01	1.3	573
W	~0.01	1.2	453
W5Vm	3.4	1.3	573
W5Vm	3.4	0.8	453
W5Vs	2.6	1	573
W5Vs	2.6	0.7	453

3. Results

3.1. Blister formation on W grains

Fig. 1 demonstrates an interesting comparison of the D blistering formation at the W surface of different grade W materials at two exposure temperatures. The fully recrystallized rolled W sample irradiated at higher exposure temperature of 573 K, largely dense with an intermediate size blisters of ~ 0.4 μm average size, almost uniformly distributed on its surface, while lowest number of blisters with average size of ~ 0.8 μm on W grains are observed for WVm as shown in Fig. 1(a & b). Although some low dome shapes blisters are observed at surface of WVm, but most of the blisters are more like high dome spherical in shape, where irragulaty in the blister shape is observed on the surface of pure W. Fig. 1c shows unevenly distributed relatively small size of blisters with an average size of ~ 0.2 μm on W grains for WVs target sample irradiated at same temperature. Comparatively the blisters density is higher than WVm and lower than rolled W.

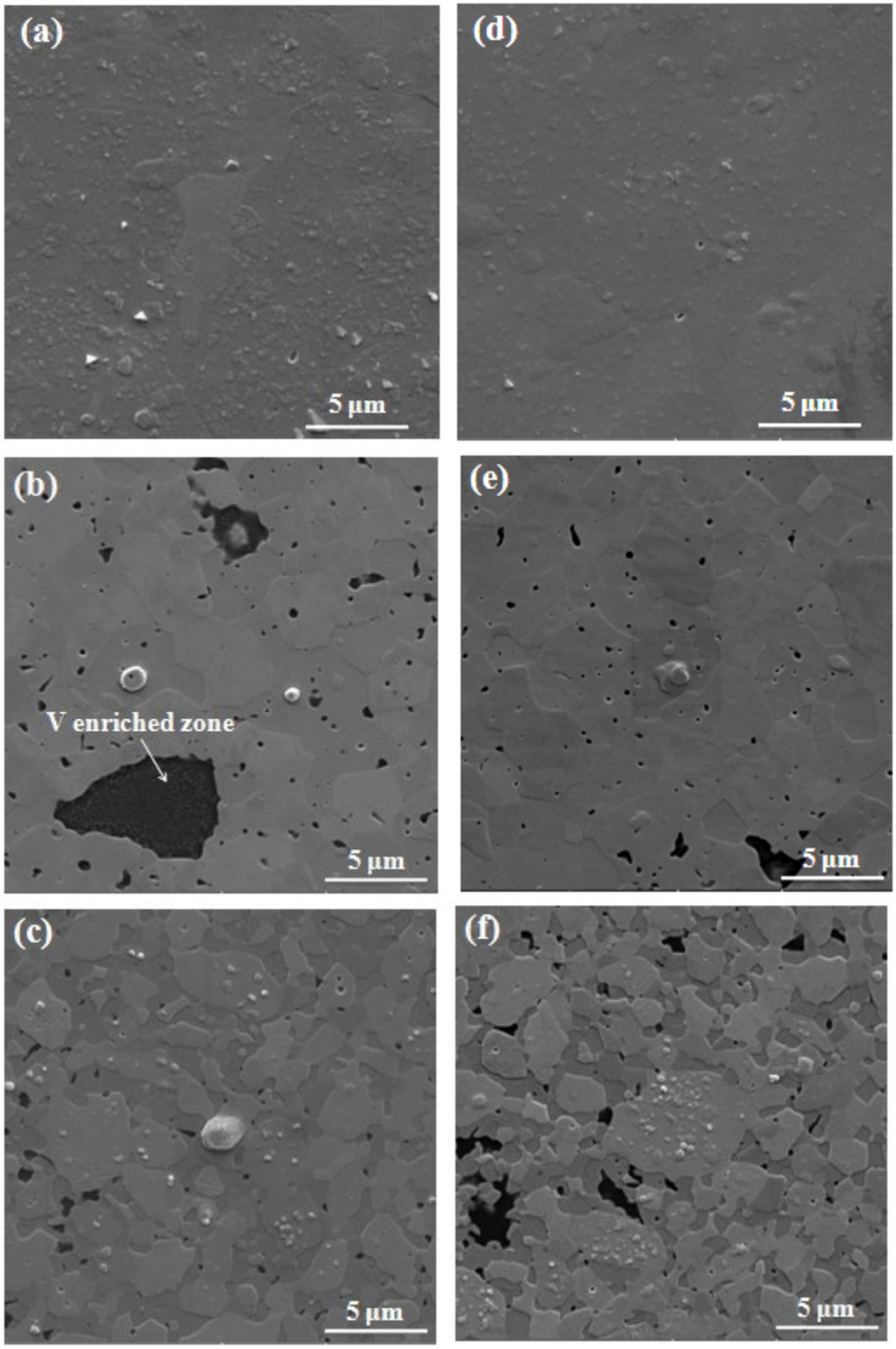

Fig. 1: Surface morphology of micron and submicron V precursor size W-V alloys (a) blisters at W surface of pure W irradiated at 573K, (b) blisters at W surface of W5Vm

irradiated at 573K, (c) blisters at W surface of W5Vs irradiated at 573K, (d) blisters at W surface of pure W irradiated at 453K, (e) blisters at W surface of W5Vm irradiated at 453K and (f) blisters at W surface of W5Vs irradiated at 453K.

At temperature of 453 K, only few blisters are observed at the W grain surface for WVm, as shown in Fig. 1e. Furthermore, the size and shape of the blisters are enterially different from the same sample tested at higher temperature. The shape of the blisters are more like low dome shape with average blister size is ~ 0.5 μm. WVs sample tested at this temperature, showing higher number density of low dome small size blisters at the W surface (Fig. 1f). However, the size of the blisters at the W grain surface for WVs is much smaller than WVm and its average size is ~ 0.1 μm. Compariatvely highest number density of D blisters are again observed on pure W surface irradiated at lower temperature (453 K).

From SEM images, it can extract that the addition of V and its different precursor size are responsible for a considerable difference in D blistering formation at surface of W based materials. Even though the average blisters size on W surface for WVm samples is relatively large but its number density is very low as compared to WVs for both temperatures. This difference in blistering formation is due to its surface morphology, which may be influenced by the difference in V precursor size. The target samples are prepared by SPS following mechanical alloying route. High energy ball miller (HEBM) promotes uniform distribution of V in W, however it is proven that due to the high ductility of V it quite difficult to reduce its size by HEBM[33]. Further, due to low sintering temperature (1873 K) and short dwell time (3min) of SPS is also not able to promote the diffusion of V in W. Consequently, most of V in W retains its individual properties up to

some extent, especially for WVm samples. Comparatively, submicron V-containing samples shows high tendency of fine V particle diffusion and alloying formation in W.

Due to the difference in V particle size the surface morphology of alloyed samples are quite different and a large plane misorientation is observed for WVs as compared to WVm as show Fig. 1. This indicates the blistering behaviour is definitely influenced by surface morphology and plane orientation. Shu et al.[34] observed similar finding of morphology dependency of blisters formation for pure W samples. In their comparative studies the blistering occurs more significantly on un-crystallized W and single crystal (111) than fully recrystallized W. Similar results about helium irradiation dependency on plane orientation are also presented by Yuan et al.[35]. The surface orientations near (0 01) plane were least affected, near (011) were medium, and the ones near (111) suffered greatest damage due to helium blisters. Hence, the surface orientation of target samples plays an important role in the formation and suppression of blisters, which is also observed in our studies for W-V alloys. This may be the reason of large number density of blisters on WVs. However, when the results of the alloys are compared with fully recrystallized rolled W irradiated under similar condition, the blistering occur more significantly on fully recrystallized rolled W than both kinds of W-V alloys. This reflects the fact that besides the blisters dependency on plane orientation, the addition of V is the most influential factor towards suppression of D blisters.

3.2. Blister formation on V enriched surface

Fig. 2 shows the blisters formation behaviour on V enriched phase at higher exposure temperature of 573 K. The blister shapes are quite irregular and their sizes are large for WVm (Fig. 2a), where most of blisters at the V enriched surface of WVs are very small

and are nearly spherical in shape as shown in Fig. 2b. Furthermore, the blisters on V particles for WVs are also uneven and even no blisters are observed on some region of single V enriched particle. Hence, the number density of D blisters on V particle is higher for WVm than WVs. Similarly, the samples exposed to low energy D at lower exposure temperature of 453 K shows replicated comparable results, with only difference of no blister on V surface of WVs. As discussed that due to the high ductility of V it is quite difficult to reduce its size by HEBM[33]. Consequently, the surface area of V in WVm is much larger than WVs. The large sizes and high number density of D blisters on V particles of WVm can be explained by the exposure of large surface area of V to D irradiation. Due to its large area exposure the chance of D blistering is enhances on the surface of V particles. Moreover, hydrogen dissolves easily in V due to negative formation energy in comparison with positive formation energy of W[36], which is the main reason for dense and large size blisters formation on V enriched surface of WVm.

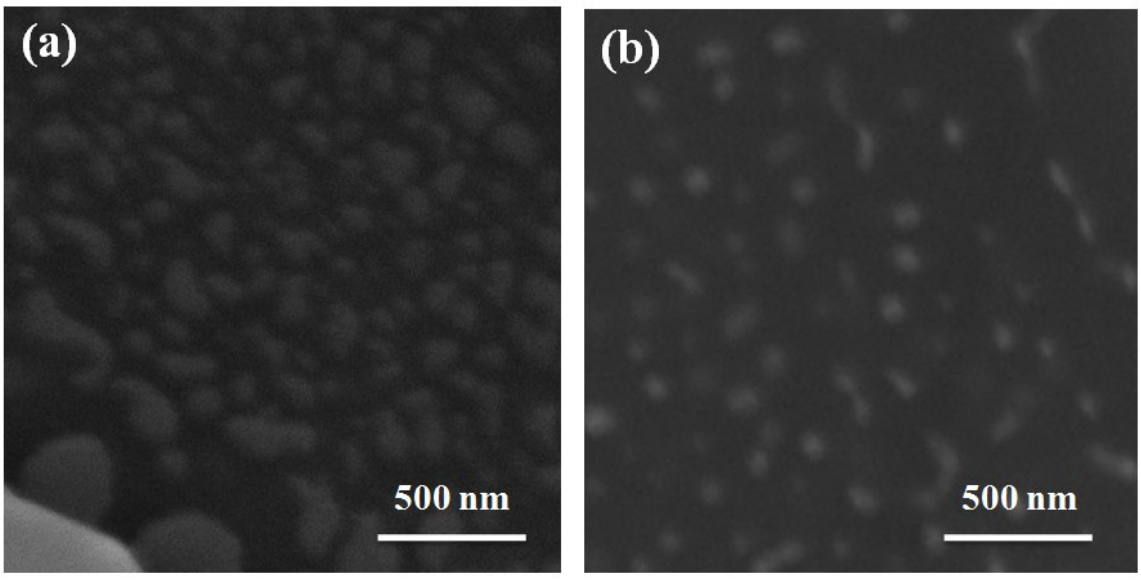

Fig. 2: Surface morphology of micron and submicron V precursor size W-V alloys (a) blisters at V surface of W5Vm irradiated at 573K and (b) blisters at V surface of W5Vs

irradiated at 573K.

3.3. Orientation dependence of blistering

Fig. 3 shows the D blistering dependency on plane orientation for WVs sample exposed to 0.9 $\times 10^{26}$ D^{+} m^{-2} at 573 K, for which D blisters is highest. The blisters are not appeared uniformly over the whole surface. Some W grains have no visible blisters but others are densely covered with blisters. Fig. 3 demonstrates the detail scheme of blisters distribution on different plane orientations for WVs. Fig. 3a shows the EBSD image of WVs, where Fig. 3b illustrates the SEM image of the same area to identify the grains with blisters. Orientation dependence of blistering can be connected with the fact that at the W surface the grains with orientation (111) are most subjected to blistering in comparison with grains of other orientations[34, 35, 37]. Our EBSD evaluations revel similar results as most of the blisters are observed near (111), where a low index plane (001) shows stability against irradiation and indicates to be less influenced by D fluence. Hence, the plane orientation dependency of blisters is not affected by V addition to W.

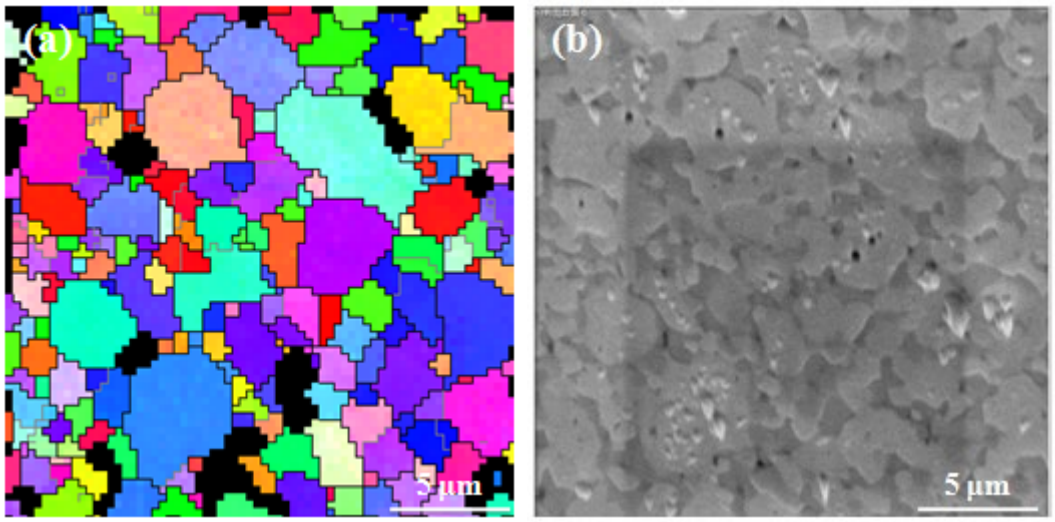

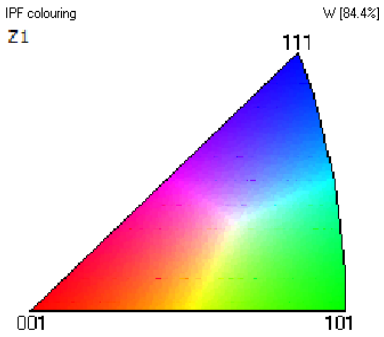

Fig. 3: D blistering dependency on plane orientation for W5Vs irradiated at 573K (a) EBSD image and (b) SEM image of the same area.

3.4. Internal features of the blisters

In order to observe the internal characteristics of D blisters at W surface, cross section of the blister is fabricated by FIB and its image is captured by SEM. Figure 4a shows the cross sectional view of large blisters at WVs surface exposed to the fluence of 0.9×10^{26} D/m^2 at 573 K. A large cavity of about 750 nm in diameter and 170 nm in height, produced by D blistering with a skin thickness of about 350 nm as given in figure 4a. The ratio of height to width of the blister is observed about 0.7. Furthermore, no cracks or voids are observed at grain boundaries as reported before [38].

FIB analysis of two relatively small identical blisters at different location of the same sample as shown in Fig. 4b. The height to width ratio of these blisters is slightly larger than big blister as show in Fig. 4a. Similarly, the ratio of height to width of these blisters is observed about 0.9 and 0.8, which is also slightly higher than the bigger blister. For tungsten like materials irradiated with low energy D plasma such as at energies below the displacement threshold, the mechanism of plastic deformation due to D super-saturation is responsible for formation of trapping sites for D [39]. During high flux D plasma, the

amount of D concentration in the irradiated area exceeds the solubility limit and produce stresses in the matrix lattice until plastic deformation occurs to stabilize these tensions.

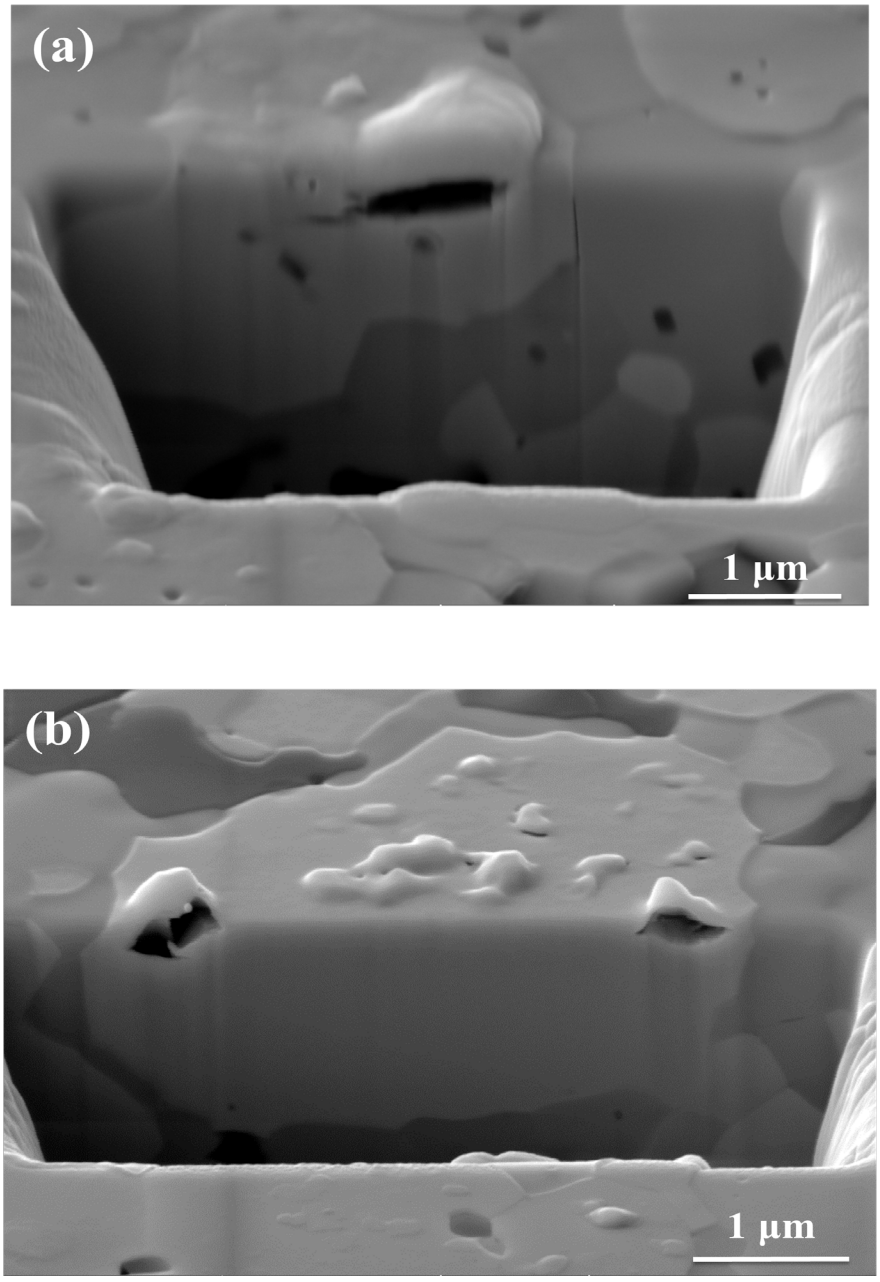

Fig. 4: FIB analysis of W5Vs irradiated at 573K (a) internal feature of the large blister and (b) internal feature of two identical relatively small blisters.

This deformation is considered to generate different defeats like vacancies and

microscopic cavities to accumulate the diffusing D. Our SEM images of the FIB cut section show a clear evidence of plastic deformed cavities produced during D exposure. Furthermore, the grain boundaries are quite clean and no cracking is observed on it. In addition V tries to occupy porosity on the grain boundaries [26] and provides stability to grain boundaries against cracking during D irradiation. Moreover, unlike D trapping initiated by carbide precipitates in W-TiC and W-TaC as discussed by Zibrov et al.[40], the diffused V particles in W do not show as trapping sits for D. Thus grain boundaries are not responsible for any of these cavities.

3.5. D retention

Fig. 5 shows the TDS spectrum of different irradiated samples at two different temperatures. The surface temperature of irradiated sample is roughly Gaussian due to the inherent non-uniformity of the plasma beam generated by Polit PSI, as discussed in Ref. [15]. However, the maximum values of surface temperature of irradiated samples measured by infrared camera are presented here. For WVm samples, one desorption peak can be distinguished located at about 470 K, with a long desorption tail along higher temperatures (673-1173 K). A higher exposure temperature of 573 K results in a larger peak at 490 K and a longer tail at high temperatures for the same sample. The D desorption in W5Vm exposed at 573 K is not finished when the maximum surface temperature (1173 K) is reached during TDS. For WVs samples one desorption peak at 423 K with a shoulder at higher temperature is observed. Again a higher exposure temperature results in a higher desorption peak and an elongated shoulder.

The increase in exposure temperature, leads to a shift of the desorption peaks toward higher temperatures and increase the net amount of retained D for both kinds of alloy

samples. Although the targets are fabricated from the same metallurgical rout, but due to the difference of V precursors powder size, the porosity level of WVm (3.4%) is slightly higher than WVs (2.6%), implies more defects and vacancies in WVm. These defects in metals are the most attractive location for D trapping, which eventually cause the macroscopic deformation and failure mechanisms observed in a variety of metals[40]. In the previous investigations, a strong interaction of H isotopes with vacancy-type defects in W[41-46] and V[36, 46] have been found. For example, the vacancy in W and V is shown to easily trap H atoms and the trapping energy in case of pure W is favorable at least six H atoms[43], where for pure V metal is up to six H atoms[46] or twelve H atoms[36] . Furthermore, H atoms also assist vacancy formation in metals such as Ni, Cr and Pd[47], which cause further enhance of the H retention.

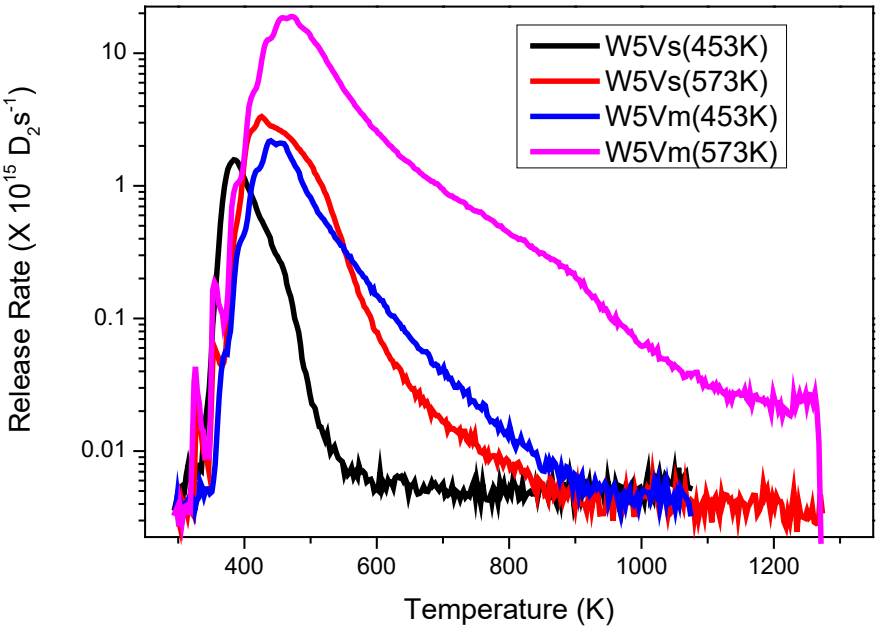

Fig. 5: Comparison between TDS spectra of D release rate of the irradiated samples at different irradiated temperature.

The TDS results indicate that the high porosity level of WVm targets show attraction for D accumulation, which is similar to the behavior of H in V, W and other BCC metals[48]. Such strong trapping between H isotopes and vacancies indicates that vacancies act as efficient trapping centers, which would drive large amounts of D to segregate towards the vacancies. Furthermore, the accumulated large amounts of D concentration at these defects are responsible for such higher D retention peak for WVm irradiated at higher temperature as reported by Golubeva et al for W and W-Re alloy[49].

The abnormal height of WVm TDS peak may not only to its morphology, exposure temperature but also due to higher fluence of 1.3×10^{26} D/m^2 as shown in Table 1. The TDS peak of WVm at lower exposure temperature of 453 K is higher than D retention peak of WVs at same irradiated temperature, but slightly lower than WVs target exposed to higher exposure temperature. Hence, besides the influence of the defects in the target materials, the effect of irradiation temperature cannot be ignored. This illustrates the formation of additional high energy traps in W-V targets at 573 K, may be due to the moment and agglomeration of vacancies. A similar tendency in shift of TDS peaks towards higher temperatures was also observed for different grade W materials[50, 51]. A slight difference between the temperatures of the TDS peaks of different grades W-V target can be seen in Fig. 5. The reason for this difference may be morphology of the different grade targets. However, all of these peaks fall in the low-temperature peaks regime of TDS spectra, which tribute to deuterium release from natural defects[5050].

4. Conclusions

D retention and blistering behavior in fully recrystallized rolled W and different size

V-containing W-V alloys were exposed to low energy and high-flux D plasma at two different temperatures (453 K and 573 K). W-V targets of micron and submicron V precursor's size powder were fabricated by spark plasma sintering. It was found that blister characteristics strongly depended on V precursor's size and surface morphology of the targets. Different blisters with different shapes and size were observed for different grades samples. SEM images revealed a more significantly blisters formation at the surface of fully recrystallized rolled W. lowest tendency of blistering formation was observed for micron V-containing targets. The blisters formation on W surface of submicron V-containing samples was mostly distributed near (111) plane. To retrieve the blistering formation mechanism, focused ion beam analyses were used. No blisters were observed on the grain boundaries and the diffused V particles in W were not responsible for D blistering formation. The amount of D retained in irradiated submicron V-containing materials was found to decrease significantly as compared with micron V-containing targets analyzed by thermal desorption spectroscopy. Blisters on V enriched surface have also been reported for both alloys. D blistering and retention was very low for both kinds of samples irradiated at lower exposure temperature of 453 K, where most D atoms were detrapped and desorbed. At higher exposure temperature of 573 K, maximum D retention was observed for micron V-containing sample due to a large occupancy of D over many trap sites.

Acknowledgments

This work was supported by National Magnetic Confinement Fusion Science Program of China under Grant 2013GB109003, China National Funds for Distinguished Young

Scientists and Higher Education Commission (HEC) of Pakistan.

References

1. R. Joachim and S. Klaus, Physica Scripta **2011** (T145), 014031 (2011).
2. M. Rieth, J. L. Boutard, S. L. Dudarev, T. Ahlgren, S. Antusch, N. Baluc, M. F. Barthe, C. S. Becquart, L. Ciupinski, J. B. Correia, C. Domain, J. Fikar, E. Fortuna, C. C. Fu, E. Gaganidze, T. L. Galán, C. García-Rosales, B. Gludovatz, H. Greuner, K. Heinola, N. Holstein, N. Juslin, F. Koch, W. Krauss, K. J. Kurzydlowski, J. Linke, C. Linsmeier, N. Luzginova, H. Maier, M. S. Martínez, J. M. Missiaen, M. Muhammed, A. Muñoz, M. Muzyk, K. Nordlund, D. Nguyen-Manh, P. Norajitra, J. Opschoor, G. Pintsuk, R. Pippan, G. Ritz, L. Romaner, D. Rupp, R. Schäublin, J. Schlosser, I. Uytdenhouwen, J. G. van der Laan, L. Veleva, L. Ventelon, S. Wahlberg, F. Willaime, S. Wurster and M. A. Yar, Journal of Nuclear Materials **417** (1–3), 463-467 (2011).
3. Z. Zhou, Y. Ma, J. Du and J. Linke, Materials Science and Engineering: A **505** (1–2), 131-135 (2009).
4. G. A. Cottrell, Journal of Nuclear Materials **334** (2–3), 166-168 (2004).
5. H. Bolt, V. Barabash, W. Krauss, J. Linke, R. Neu, S. Suzuki, N. Yoshida and A. U. Team, Journal of Nuclear Materials **329–333, Part A** (0), 66-73 (2004).
6. P. Gumbsch, Journal of Nuclear Materials **323** (2–3), 304-312 (2003).
7. D. F. Johnson and E. A. Carter, Journal of Materials Research **25** (02), 315-327 (2010).
8. M. Faleschini, H. Kreuzer, D. Kiener and R. Pippan, Journal of Nuclear Materials **367–370, Part A** (0), 800-805 (2007).

9. J. Martínez, B. Savoini, M. A. Monge, A. Muñoz, D. E. J. Armstrong and R. Pareja, Fusion Engineering and Design **88** (9–10), 2636-2640 (2013).
10. T. Palacios, J. Y. Pastor, M. V. Aguirre, A. Martín, M. A. Monge, A. Muñóz and R. Pareja, Journal of Nuclear Materials **442** (1–3, Supplement 1), S277-S281 (2013).
11. M. Rieth and B. Dafferner, Journal of Nuclear Materials **342** (1–3), 20-25 (2005).
12. B. M. Savoini, J.; Muñoz, A.; Monge, M. A.; Pareja, R., Journal of Nuclear Materials **442** (1–3), S229-S232 (2013).
13. J. Hohe and P. Gumbsch, Journal of Nuclear Materials **400** (3), 218-231 (2010).
14. A. Muñoz, M. A. Monge, B. Savoini, M. E. Rabanal, G. Garces and R. Pareja, Journal of Nuclear Materials **417** (1–3), 508-511 (2011).
15. Y. Zayachuk, M. H. J. t. Hoen, I. Uytdenhouwen and G. V. Oost, Physica Scripta **2011** (T145), 014041 (2011).
16. Y. Zayachuk, M. H. J. t. Hoen, P. A. Z. v. Emmichoven, I. Uytdenhouwen and G. v. Oost, Nuclear Fusion **52** (10), 103021 (2012).
17. J. Linke, T. Loewenhoff, V. Massaut, G. Pintsuk, G. Ritz, M. Rödig, A. Schmidt, C. Thomser, I. Uytdenhouwen, V. Vasechko and M. Wirtz, Nuclear Fusion **51** (7), 073017 (2011).
18. L. Th, A. Bürger, J. Linke, G. Pintsuk, A. Schmidt, L. Singheiser and C. Thomser, Physica Scripta **2011** (T145), 014057 (2011).
19. J. W. Coenen, V. Philipps, S. Brezinsek, G. Pintsuk, I. Uytdenhouwen, M. Wirtz, A. Kreter, K. Sugiyama, H. Kurishita, Y. Torikai, Y. Ueda, U. Samm and T.-T. the, Nuclear Fusion **51** (11), 113020 (2011).
20. Y. Mutoh, K. Ichikawa, K. Nagata and M. Takeuchi, Journal of Materials Science

30 (3), 770-775 (1995).

21. L. El-Guebaly, R. Kurtz, M. Rieth, H. Kurishita, A. Robinson and A. Team, Fusion Science and Technology **60** (1), 185-189 (2011).
22. S. Wurster, N. Baluc, M. Battabyal, T. Crosby, J. Du, C. García-Rosales, A. Hasegawa, A. Hoffmann, A. Kimura, H. Kurishita, R. J. Kurtz, H. Li, S. Noh, J. Reiser, J. Riesch, M. Rieth, W. Setyawan, M. Walter, J. H. You and R. Pippan, Journal of Nuclear Materials **442** (1–3, Supplement 1), S181-S189 (2013).
23. M. V. Aguirre, A. Martín, J. Y. Pastor, J. Llorca, M. A. Monge and R. Pareja, Metallurgical and Materials Transactions A **40** (10), 2283-2290 (2009).
24. M. V. Aguirre, A. Martín, J. Y. Pastor, J. Llorca, M. A. Monge and R. Pareja, Journal of Nuclear Materials **404** (3), 203-209 (2010).
25. S. Wurster, B. Gludovatz, A. Hoffmann and R. Pippan, Journal of Nuclear Materials **413** (3), 166-176 (2011).
26. K. Arshad, M.-Y. Zhao, Y. Yuan, Y. Zhang, Z.-H. Zhao, B. Wang, Z.-J. Zhou and G.-H. Lu, Journal of Nuclear Materials **455** (1–3), 96-100 (2014).
27. Y. Zhang, A. V. Ganeev, J. T. Wang, J. Q. Liu and I. V. Alexandrov, Materials Science and Engineering: A **503** (1–2), 37-40 (2009).
28. Y. Kitsunai, H. Kurishita, H. Kayano, Y. Hiraoka, T. Igarashi and T. Takida, Journal of Nuclear Materials **271–272** (0), 423-428 (1999).
29. K. Arshad, W. Guo, J. Wang, M.-Y. Zhao, Y. Yuan, Y. Zhang, Z.-J. Zhou and G.-H. Lu, International Journal of Refractory Metals & Hard Materials ((Under review)).
30. K. Arshad, M.-Y. Zhao, Y. Yuan, Y. Zhang, Z.-J. Zhou and G.-H. Lu, Modern

Physics Letters B **28** (26), 1450207 (2014).

31. M. Gilbert and R. Forrest, *Handbook of activation data calculated using EASY-2003*. (EURATOM/UKAEA Fusion Association, 2004).
32. M. H. J. t. Hoen, B. Tyburska-Püschel, K. Ertl, M. Mayer, J. Rapp, A. W. Kleyn and P. A. Z. v. Emmichoven, Nuclear Fusion **52** (2), 023008 (2012).
33. K. Arshad, Z. Ming-Yue, Y. Yue, Z. Ying, Z. Zhen-Hua, W. Bo, Z. Zhang-Jian and L. Guang-Hong, presented at the 11th International Bhurban Conference on Applied Sciences and Technology (IBCAST) 2014 (unpublished).
34. W. M. Shu, A. Kawasuso, Y. Miwa, E. Wakai, G. N. Luo and T. Yamanishi, Physica Scripta **2007** (T128), 96 (2007).
35. Y. Yuan, H. Greuner, B. Böswirth, C. Linsmeier, G. N. Luo, B. Q. Fu, H. Y. Xu, Z. J. Shen and W. Liu, Journal of Nuclear Materials **437** (1–3), 297-302 (2013).
36. L.-J. Gui, Y.-L. Liu, W.-T. Wang, S. Jin, Y. Zhang, G.-H. Lu and J.-E. Yao, Journal of Nuclear Materials **442** (1–3, Supplement 1), S688-S693 (2013).
37. H. Y. Xu, Y. B. Zhang, Y. Yuan, B. Q. Fu, A. Godfrey, G. De Temmerman, W. Liu and X. Huang, Journal of Nuclear Materials **443** (1–3), 452-457 (2013).
38. W. M. Shu, E. Wakai and T. Yamanishi, Nuclear Fusion **47** (3), 201 (2007).
39. V. K. Alimov, J. Roth and M. Mayer, Journal of Nuclear Materials **337–339** (0), 619-623 (2005).
40. Y. Zhang, T. Ozaki, M. Komaki and C. Nishimura, Scripta Materialia **47** (9), 601-606 (2002).
41. L. Guang-Hong, Z. Hong-Bo and S. B. Charlotte, Nuclear Fusion **54** (8), 086001 (2014).

42. Y.-L. Liu, Y. Zhang, H.-B. Zhou, G.-H. Lu, F. Liu and G. N. Luo, Physical Review B **79** (17), 172103 (2009).

43. L. Sun, S. Jin, X.-C. Li, Y. Zhang and G.-H. Lu, Journal of Nuclear Materials **434** (1–3), 395-401 (2013).

44. Z. Hong-Bo, L. Yue-Lin, J. Shuo, Z. Ying, G. N. Luo and L. Guang-Hong, Nuclear Fusion **50** (2), 025016 (2010).

45. Y.-N. Liu, T. Ahlgren, L. Bukonte, K. Nordlund, X. Shu, Y. Yu, X.-C. Li and G.-H. Lu, AIP Advances **3** (12), - (2013).

46. C. Ouyang and Y.-S. Lee, Physical Review B **83** (4), 045111 (2011).

47. Y. Fukai, Physica Scripta **2003** (T103), 11 (2003).

48. Y. Tateyama and T. Ohno, Physical Review B **67** (17), 174105 (2003).

49. A. V. Golubeva, M. Mayer, J. Roth, V. A. Kurnaev and O. V. Ogorodnikova, Journal of Nuclear Materials **363–365** (0), 893-897 (2007).

50. O. V. Ogorodnikova, J. Roth and M. Mayer, Journal of Applied Physics **103** (3), 034902 (2008).

51. M. Zibrov, M. Mayer, E. Markina, K. Sugiyama, M. Betzenbichler, H. Kurishita, G. Yu, O. V. Ogorodnikova, A. Manhard and A. Pisarev, Physica Scripta **2014** (T159), 014050 (2014).